VIV-galloping instability of a rectangular cylinder in turbulent flow

Claudio Mannini[1], Antonino M. Marra[1], Tommaso Massai[1], Gianni Bartoli[1]
[1]CRIACIV/ Department of Civil and Environmental Engineering, University of Florence, Florence, Italy
email: claudio.mannini@dicea.unifi.it, antonino.marra@dicea.unifi.it, tmassai@dicea.unifi.it, gianni.bartoli@unifi.it

ABSTRACT: The phenomenon of interference of vortex-induced vibration (VIV) and galloping was studied in the case of a slender rectangular cylinder with a side ratio of 1.5 and the short side placed perpendicular to the flow. In particular, in this paper the effect of turbulence was considered, by generating several homogeneous turbulent flows with different turbulence intensities and the integral length scales. Two section models were considered differing for the aspect ratios, the nondimensional mass and the reference Reynolds number. Very different behaviors were observed in smooth flow for the two models: the larger model showed a strong proclivity to a combined VIV-galloping instability, while the smaller one seemed to follow in a very accurate way the quasi-steady prediction. The experiments showed that the galloping instability, either interacting with vortex shedding or not, is delayed by turbulence to higher flow speeds but the section became stable in the observable wind velocity range only for high turbulence intensity and large integral length scale. Limiting so far to the case of the larger section model in smooth flow, the dependence of the dynamic response on the dissipation capability of the mechanical system was explored by progressively varying the damping in a controlled way through magnetic damper devices.

KEY WORDS: Galloping; Vortex-Induced Vibrations; Rectangular Cylinder; Wind Tunnel Tests; Turbulent Flow.

1 INTRODUCTION

Slender prismatic and nearly-prismatic bodies characterized by a bluff cross section with sufficient afterbody are prone to both vortex-induced vibrations (VIV) and galloping. Galloping instability in the transverse degree of freedom usually occurs at high reduced wind speed and is therefore approached with the quasi-steady theory. By contrast, vortex-induced vibration is typically a low reduced wind speed, fully unsteady, phenomenon (Figure 1). Nevertheless, if the oscillating structure is light and low damped, three important consequences can ensue: i) vortex-induced vibrations are supposed to occur with larger amplitudes in a wider range of flow speeds; ii) VIV and galloping are supposed to onset at close flow speeds and may interact with each other; iii) the quasi-steady theory could fail to predict the galloping instability threshold and the post-critical oscillatory behavior, due to the not-high-enough reduced wind speed.

In particular, in the case of rectangular cylinders with side ratios B/D lower than, say, about 3, being B and D respectively the streamwise and cross-flow section dimensions, a combined VIV-galloping instability can easily occur in the transverse mode. This phenomenon features sustained vibrations starting at the Kármán-vortex resonance flow speed, similarly to VIV, but with amplitudes continuously growing with the flow speed, as typical for galloping (Figure 1). As shown by a recent literature survey [1], an instability with these characteristics can occur even when the theoretical galloping critical wind speed (calculated with the quasi-steady theory) is significantly larger than the resonance wind speed, *i.e.*, for relatively high values of nondimensional mass and mechanical damping of the system. This behavior implies large-amplitude oscillations where they are not predicted by the classical theories, with important consequences from the practical engineering point of view. The inadequacy with respect to this issue of the present international codes and recommendations has already been underscored [1].

In some previous works [1-3] the authors experimentally studied the VIV-galloping instability in the transverse degree of freedom of a rectangular cylinder with a side ratio of 1.5, placed perpendicularly to the smooth flow with zero angle of attack. In fact, this two-dimensional body exhibited a strong proclivity to the interaction between Kármán-vortex shedding and galloping. Numerical calculations with two analytical models available in literature were also carried out in Ref. [4].

In this paper, the same cylinder is considered to investigate the role played by turbulence on this interaction phenomenon. In addition, the effect of progressively varying the damping of the system in a controlled way through magnetic damper devices was explored, though so far only in smooth flow.

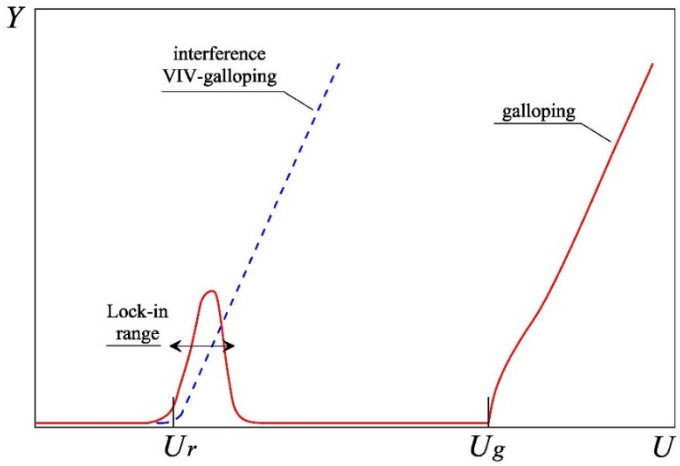

Figure 1. Comparison between classical behavior with separated VIV and galloping excitations (solid line) and instability due to the interference between the two phenomena (dashed line).

2 WIND TUNNEL TESTS

2.1 Wind tunnel facility and models

The tests were carried out in the open-circuit boundary-layer wind tunnel of CRIACIV in Prato, Italy. The facility is about 22 m long and presents at the inlet a convergent with a contraction ratio of 3 to 1 after the honeycomb and a T-diffuser at the outlet. The rectangular test section is 2.42 m wide and 1.60 m high. Air is aspired through a motor with a nominal power of 156 kW and the flow speed can be varied continuously up to 30 m/s by adjusting through an inverter the rotation speed of the fan or the pitch of the ten blades of it. In the absence of turbulence generating devices, the free-stream turbulence intensity is around 0.7%.

First, a plywood sectional model, 986 mm long (L), 116 mm wide (B) and 77 mm deep (D), identified in the following as D77, was used to perform both static and dynamic tests. To enforce bidimensional flow conditions, symmetric rectangular plates in plywood were provided at the model ends; their dimensions (450 mm × 150 mm × 4 mm) were designed according to the principles reported in Ref. [5]. The mass of the model, end-plates and supporting carbon-fiber tube was 1.730 kg. Afterwards, the tests were repeated on an aluminum model, 1 m long, 45 mm wide and 30 mm deep, identified in the following as D30. In this case, rectangular aluminum end plates (150 mm × 90 mm × 1.5 mm, the long side extending 15 mm upstream the downward face and 90 mm downstream the leeward face) were provided for the aeroelastic tests, while circular steel end plates with a diameter of 300 mm were employed for the static tests. The total mass of the model was 2.352 kg. Both models were placed horizontally in the wind tunnel with the shorter side of the section perpendicular to the flow. The blockage ratio was 4.8% for the plywood model and 1.9% for the aluminum model.

The homogeneous turbulent flow was generated by two different wooden grids placed at various distances upstream of the model (Figure 1), in a way similar to that followed by Laneville [6]. Grid #1 was characterized by a mesh of 100 mm × 100 mm with slats of a depth of 25 mm, while grid #2 by a mesh of 550 mm × 550 mm with slats of 140 mm. The spectral properties of the induced turbulence were determined through measurements with a Dantec single-component hot-wire probe 55P11 connected to a Dantec CTA 56C01 module and a 56C17 bridge. The spatial homogeneity of the flow at the position of the model was verified prior to start the tests. The various configurations considered are listed in Tables 1 and 2, which also report the turbulence intensity and the longitudinal integral length scale. The latter was calculated according to Taylor's frozen-eddy hypothesis and the results were confirmed by adapting a von Kármán spectrum to the measured spectrum (see Figure 3 for three examples of measured and fitted power spectral density). It is worth noting that in all configurations the turbulence intensity tends to moderately increase with the flow mean speed.

The mean flow speed was monitored with a Pitot tube placed 3.5 m upstream of the model and connected to a sensor Setra AccuSense model ASL. Prior to place the model in the wind tunnel, the conversion coefficient between the mean wind speed registered by the reference Pitot tube and that measured at the midspan of the future model location was determined for each wind speed and free-stream turbulence considered.

2.2 Static set-up

The measurement of the aerodynamic force coefficients at various angles of attack and of the Strouhal number were performed by means of two high-frequency six-components strain-gauges dynamometers ATI FT-Delta SI-165-15 placed one at each end of the model. The dynamometers were supported by two rigid steel frames jutting out from two steel columns. The flow angle of attack was manually adjusted by means of an inclinometer DXL360S with an accuracy of 0.05°.

2.3 Aeroelastic set-up

In the aeroelastic setup the model was connected through its longitudinal axis-tube to two shear-type steel frames, the horizontal elements of which worked as plate-springs. Only the transversal displacement was allowed by the two frames due to the very large in-plane bending stiffness of the vertical elements at which the model was connected. The aerodynamic damping due to the exposition to the flow of the plate-springs was verified to be very small.

The displacements of the model were recorded respectively with two non-contact laser transducers Micro-epsilon OptoNCDT 1605. The damping and frequency of the system were measured imposing several times an initial condition and recording the free decay of the oscillations. Theoretically the damping should be measured in the void and the contribution of still air is slightly nonlinear and increases with the amplitude of the oscillation. Consequently, this effect was minimized by considering small vibrations only, with a fixed maximum amplitude of 0.5 mm. The effective mass of the oscillating system was calculated from the measurement of the static stiffness of the system (17709 N/m).

Figure 2. Grids used to generate turbulence: grid #1 (left) and grid #2 (right).

Table 1. Turbulent flow and dynamic characteristics of the aeroelastic tests performed with the plywood model (D = 77 mm). Δx denotes the distance between the grid and the longitudinal axis of the model, I_u the turbulence intensity, L_u^x the longitudinal turbulence length scale. ζ_0 is the ratio-to-critical mechanical damping of the system and $m^* = \rho D^2 L/M$ is the mass ratio, where M = 4.77 kg is the effective mass of the system and ρ the air density. $Sc = 4\pi \cdot M \cdot \zeta_0 / \rho BD$ is the Scruton number and $U_g = 2Sc/A_1 \cdot n_0 B$ is the quasi-steady galloping critical wind speed, calculated for a slope of the transverse force coefficient $A_1 = dC_{Fy}/d\alpha(0) = 4.9$ (Figure 5); $Re_r = \rho U_r D/\mu$ is the Reynolds number corresponding to the vortex-resonance wind speed U_r. The frequency of transverse vibration was n_0 = 9.70 Hz.

Test	Grid	Δx [m]	I_u [%]	L_u^x/D [-]	ζ_0 [%]	m^* [-]	Sc [-]	U_g/U_r [-]	Re_r [-]
D77-1	no grid	-	1	-	0.088	7.2e-04	5.1	0.28	36,200
D77-2	#1	4.95	3	1.0	0.086	7.2e-04	4.9	0.27	36,200
D77-3	#1	1.50	6	0.6	0.096	7.2e-04	5.5	0.31	36,200
D77-4	#1	0.90	9	0.5	0.081	7.2e-04	4.6	0.26	36,200
D77-5	#1	0.70	11	0.4	0.075	7.3e-04	4.3	0.24	36,200
D77-6	#1	0.50	16	0.4	0.110	7.2e-04	6.3	0.35	36,100
D77-7	#2	6.84	9	3.3	0.072	7.2e-04	4.1	0.23	36,200
D77-8	#2	5.00	14	3.0	0.110	7.1e-04	6.4	0.35	36,100

Table 2. Turbulent flow and dynamic characteristics of the aeroelastic tests performed with the aluminum model (D = 30 mm). The quasi-steady galloping critical wind speed was calculated for a slope of the transverse force coefficient $A_1 = dC_{Fy}/d\alpha(0) = 6.5$ (Figure 6). The effective mass of the system was M = 5.42 kg and the frequency of transverse vibration n_0 = 9.10 Hz

Test	Grid	Δx [m]	I_u [%]	L_u^x/D [-]	ζ_0 [%]	m^* [-]	Sc [-]	U_g/U_r [-]	Re_r [-]
D30-1	no grid	-	1	-	0.057	9.8e-05	24.4	1.18	5200
D30-2	#1	4.95	3	2.6	0.057	9.9e-05	24.1	1.17	5200
D30-3	#1	1.50	6	1.5	0.059	9.8e-05	25.3	1.23	5200
D30-4	#1	0.90	9	1.2	0.061	9.9e-05	25.9	1.26	5200
D30-5	#1	0.70	11	1.1	0.054	9.9e-05	22.9	1.11	5200
D30-6	#1	0.50	16	0.9	0.054	9.9e-05	22.8	1.11	5200
D30-7	#2	6.84	9	8.5	0.055	9.8e-05	23.7	1.15	5200
D30-8	#2	5.00	14	7.7	0.061	9.9e-05	26.0	1.26	5200

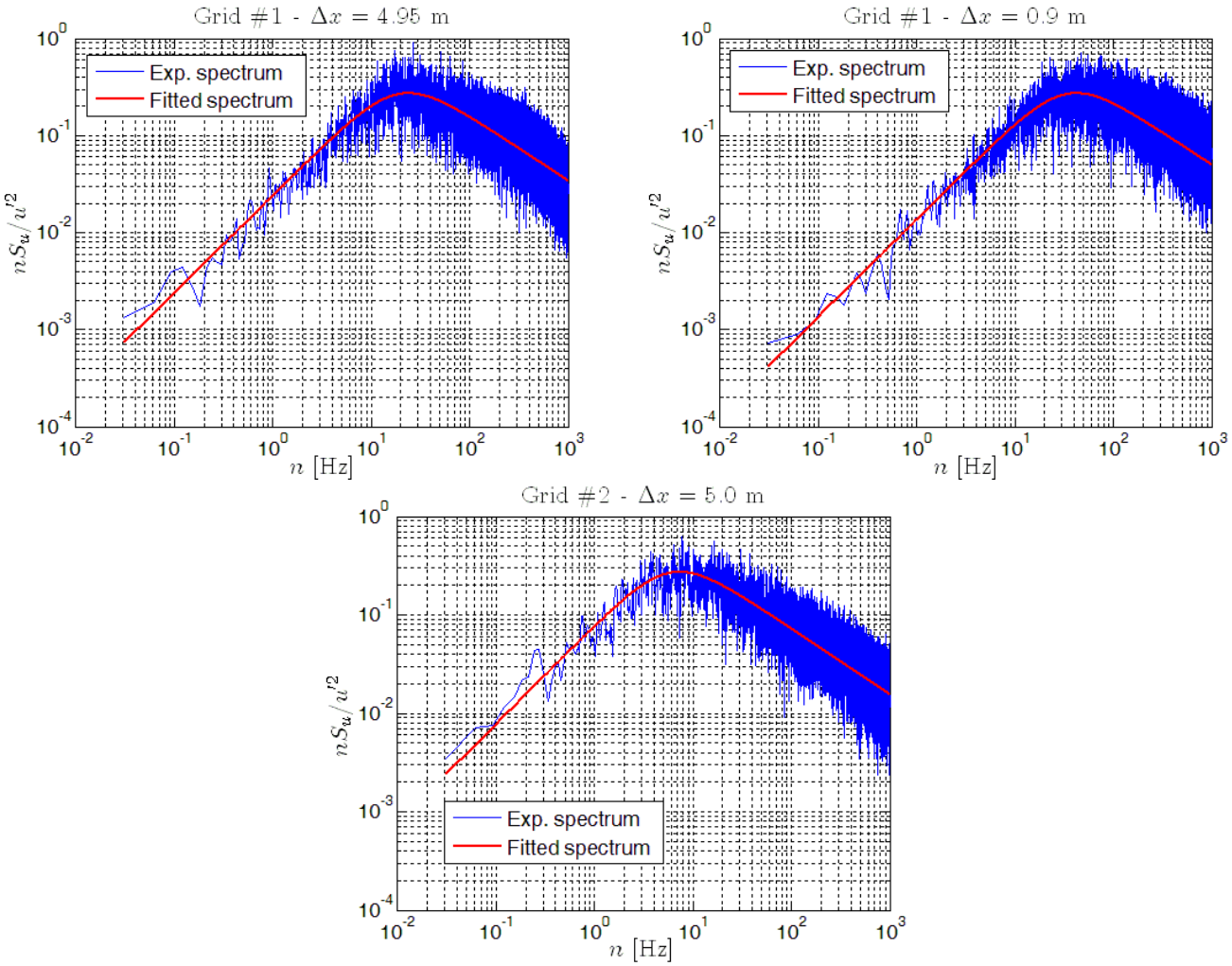

Figure 3. Normalized power spectral density of longitudinal turbulence fluctuations measured with the hot-wire anemometry for three configurations tested (see Table 1 and Table 2).

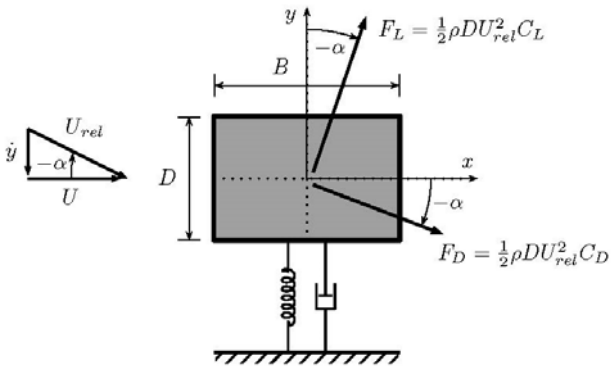

Figure 4. Evaluation of the transverse force on a vibrating rectangular cylinder with the quasi-steady approach. U_{rel} denotes the apparent flow speed due to the body displacement velocity.

3 RESULTS

3.1 Static results

According to the quasi-steady theory, the forces exerted by the flow on an oscillating body can be calculated at each time instant as if the body was stationary and invested by the apparent steady flow, as shown in Figure 4. Therefore, the transverse force coefficient acting on a slender prismatic structure can be calculated as follows:

$$C_{Fy}(\alpha) = sec(\alpha) \cdot [C_L(\alpha) + C_D(\alpha) \cdot tg(\alpha)] \tag{1}$$

where

$$\alpha = -arctg\left(\frac{\dot{y}}{U}\right) \tag{2}$$

being y/D is the nondimensional amplitude of oscillation, U the undisturbed flow speed; the dot denotes differentiation with respect to time t. C_{Fy} was determined in smooth flow at various angles of attack α for both the plywood and the aluminum model from the measurements of drag and lift coefficients. This coefficient is crucial for the prediction of the galloping instability through the quasi-steady theory [7-8]. Figure 5 and Figure 6 report a few examples of the results; the slope of the coefficient for $\alpha = 0°$, to which the quasi-steady galloping critical wind speed is inversely proportional, is highlighted. The symmetry of the measured curves with respect to the angle of attack is also apparent. The slope of the transverse force coefficient seems to be higher for the aluminum model and tends to increase with the Reynolds number. However, this parameter is known to be very sensitive to flow and geometry conditions [1] and can be non-negligibly influenced by small measurement errors. From this standpoint, it is worth keeping in mind that, generally speaking, measurements at higher wind speed tend to be more accurate and reliable, as the aerodynamic forces are larger.

In addition, from the power spectral density of the lift coefficient at various wind speeds it was possible to estimate the Strouhal number, which resulted to be 0.106 in the case of the plywood model and 0.105 for the aluminum model.

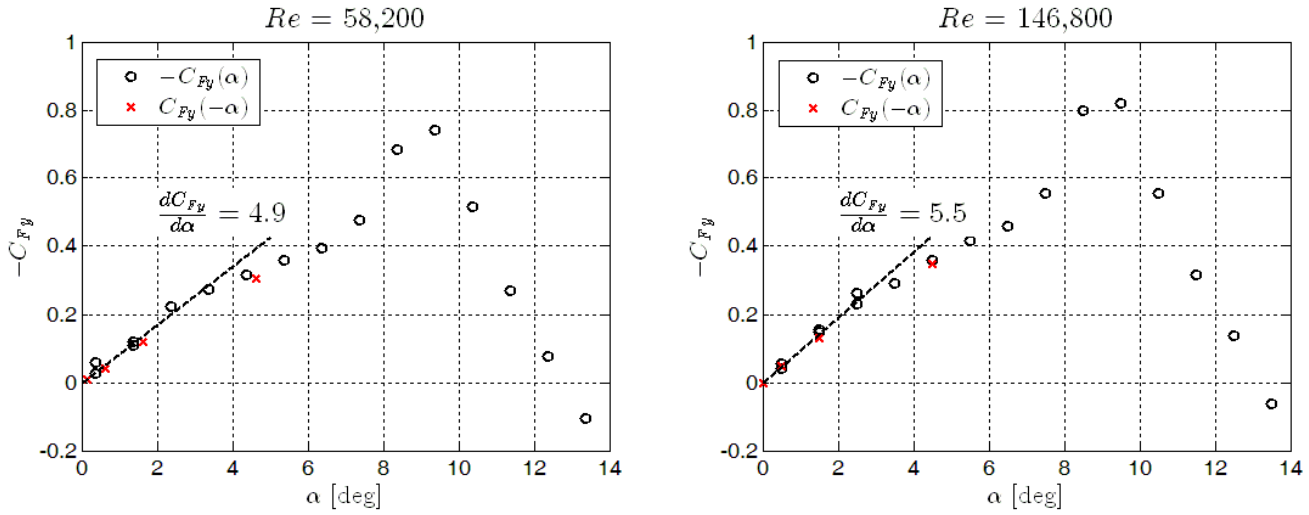

Figure 5. Transverse force coefficients measured at various angles of attack for the plywood (D = 77 mm) model. Two different values of the Reynolds number are considered. The slope in the origin was calculated for $|\alpha| \leq 2°$.

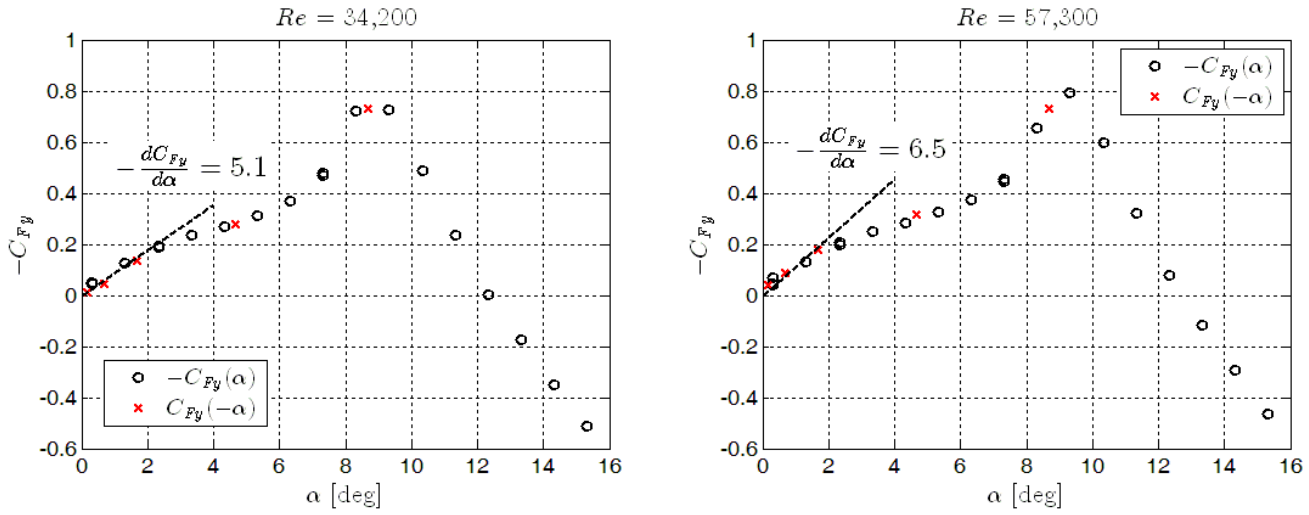

Figure 6. Transverse force coefficients measured at various angles of attack for the aluminum model (D = 30 mm). Two different values of the Reynolds number are considered. The slope in the origin was calculated for $|\alpha| \leq 1°$.

3.2 *Aeroelastic results in smooth and turbulent flow*

A crucial dynamic nondimensional parameter is the Scruton number, which accounts for the dissipation capabilities of the mechanical system. In this paper, it is defined as follows:

$$Sc = \frac{4\pi \cdot M \cdot \zeta_0}{\rho B D L} \tag{3}$$

where M is the effective mass of the system (including the contribution of the elastic suspension system), ζ_0 is the ratio-to-critical mechanical damping and ρ the air density. For the small Scruton numbers considered here, the galloping critical wind speed predicted by the quasi-steady theory is well below the Kármán-vortex resonance wind speed (about $0.3 \cdot U_r$ in smooth flow, where $U_r = n_0 D/St$, n_0 is the frequency of transverse vibration and St the Strouhal number). It is also worth keeping in mind that the quasi-steady galloping critical wind speed $U_g = 2Sc/A_1 \cdot n_0 B$, being $A_1 = dC_{Fy}/d\alpha(0)$, is not expected to be accurate for such low values of Scruton number, due to the full unsteadiness of the phenomenon. Then, it has just to be taken as a reference parameter to evaluate the proneness of the system to interference between VIV and galloping.

The dynamic tests carried out in smooth and turbulent flow with the larger plywood model (D77) are summarized in Table 1. The results show that in smooth flow (case D77-1) a galloping-type instability starts at the resonance wind speed and the vibration amplitude unrestrictedly grows with the flow speed (Figure 7). Clearly, vortex shedding suppresses galloping until $U = U_r$ (this is the so-called "quenching" effect). Moreover, as already discussed in Refs. [1-2], a secondary instability with limited amplitudes due to superharmonic resonance can be observed in a range of wind speeds starting around $U_r/3$. A hysteresis loop is also evident in this case.

A weak turbulence intensity of about 3% (case D77-2) has no significant effects on the amplitude-velocity response curve. By contrast, higher turbulence intensities are able to delay the onset of the main instability and progressively reduce the amplitudes of the secondary instability along with the flow speed range of the excitation (cases from D77-3 to D77-6). However, the amplitude-velocity curves remain approximately parallel. In flows with a high intensity of turbulence associated with a large integral length scale (cases D77-7 and D77-8) the amplitude of vibration regularly increases with the wind speed but no proper instability is observed for $U > U_r$ (at least in the range of flow speeds reachable in the wind tunnel). It is important to stress the fact that the resonance wind speed U_r in Figure 3 is presently calculated by means of the Strouhal number measured in smooth flow. Small scales of turbulence are able to modify the aerodynamic behavior of the cross section and even to foster the reattachment of the free shear layers (see *e.g.* Refs. [9-11]), so that a non-negligible effect on the vortex-shedding frequency is expected. Nevertheless, the possible variation of the Strouhal number due to turbulence does not seem to justify the large shift of the amplitude-velocity curves observed in turbulent flow. The effect of turbulence on the transverse coefficient has also to be investigated. Moreover, it has been clarified that turbulence, especially acting as parametric excitation, can have a non-negligible effect on the quasi-steady galloping instability mechanism [12-14]. Nevertheless, the actual role played by this parametric excitation in the case of interference between galloping and vortex-induced vibration is not clear.

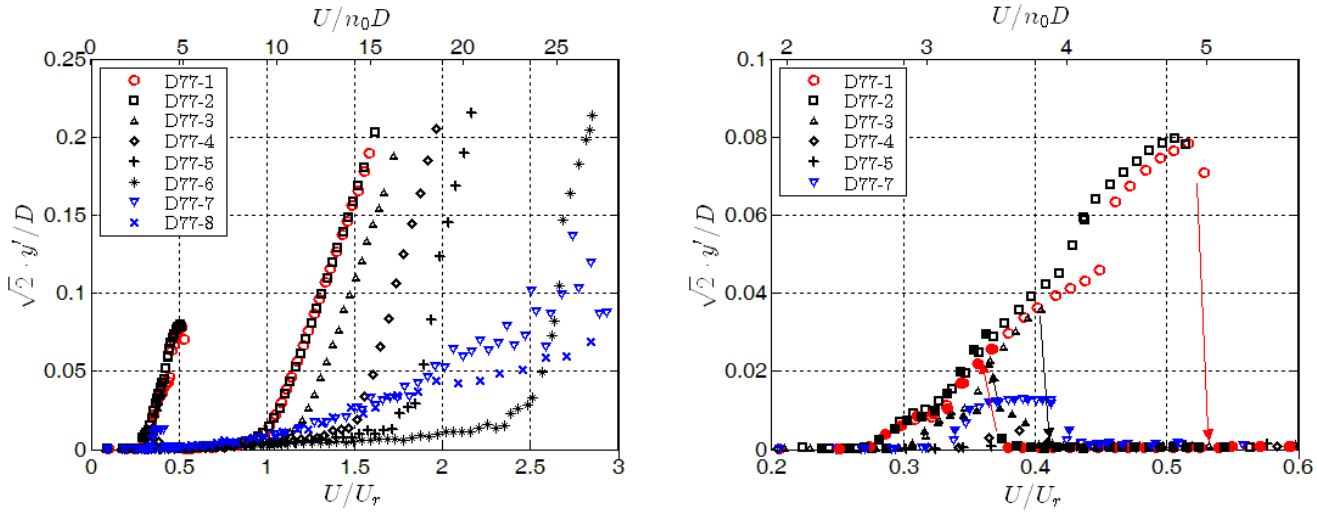

Figure 7. Aeroelastic results obtained with the wooden model (D = 77 mm) for various turbulent flow characteristics. U_r is the theoretical Kármán-vortex resonance wind speed calculated from the Strouhal number, y' denotes the standard deviation of the transverse vibration and n_0 the transverse vibration frequency of the system. The right-hand-side frame is a close-up of the left-hand-side one; the solid markers denote decreasing wind speed patterns.

The dynamic tests carried out in smooth and turbulent flow with the smaller aluminum model (D30) are summarized in Table 2. In this case, the Scruton number is significantly higher than in the previous case and therefore no excitation around $U_r/3$ is visible in Figure 8. In addition, due to the limit in the deformation attainable with the plate springs, with this model it was possible to reach much higher nondimensional amplitudes of oscillation than with the plywood one. In spite of a quasi-steady theoretical galloping critical wind speed only slightly higher than the Kármán-vortex resonance wind speed (about $1.2 \cdot U_r$ in smooth flow, case D30-1 in Table 2), no interaction between vortex shedding and galloping was observed. Moreover, the instability pattern is in very good agreement with the quasi-steady theory prediction calculated with the transverse force coefficient measured for the highest Reynolds number (Figure 6). The only exceptions are the jump to a higher branch at a wind speed slightly higher than $2 \cdot U_r$ and the small hysteresis loop around the instability threshold. This is in evident contradiction with the results of the tests with the larger plywood model, also for much higher Scruton numbers, as it will be shown in the next subsection. A possible explanation may be the effect of the Reynolds number, which was seven times smaller in the tests with the aluminum model than in those with the plywood model. Nevertheless, further investigation to explain this issue are needed.

The effect of turbulence, whose normalized integral length scale L_u^x/D is significantly larger for this model, is that of delaying the instability onset. The amplitude-velocity patterns remain similar if the integral scale of turbulence does not change much (cases from D30-2 to D30-6), while it is quite different for higher values of L_u^x/D (case D30-7). For high turbulence intensity and large integral length scale (case D30-8), the section was stable in the wind-tunnel range of flow speeds.

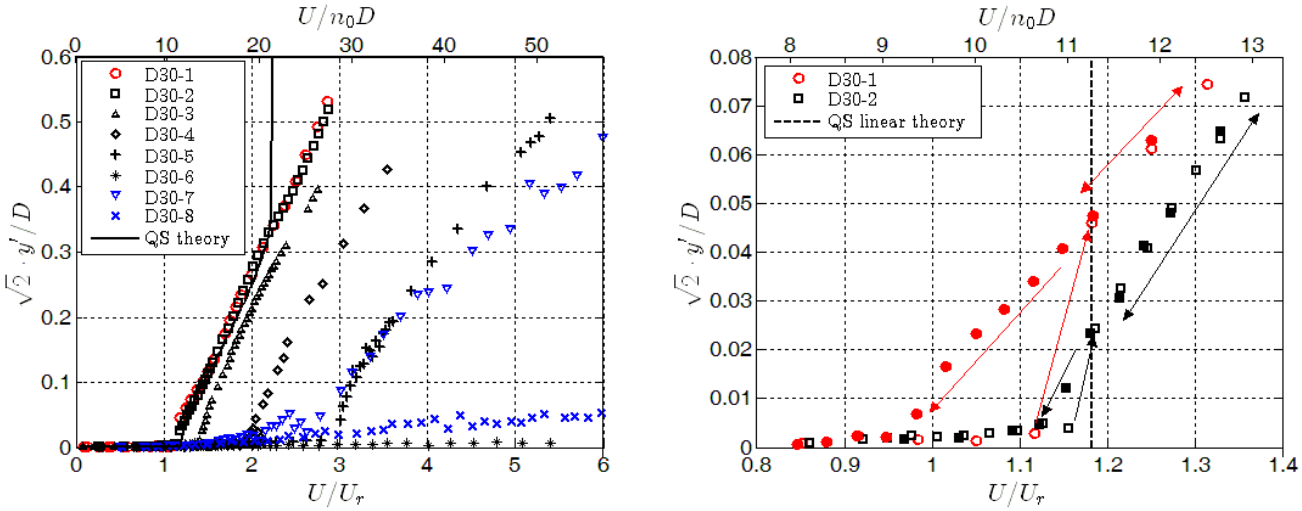

Figure 8. Aeroelastic results obtained with the aluminum model (D = 30 mm) for various turbulent flow characteristics. The right-hand-side frame is a close-up of the left-hand-side one. QS stands for "quasi-steady".

Table 3. Experimental case studies in smooth flow for the larger plywood rectangular cylinder (D = 77 mm) for various damping coefficients. The quasi-steady galloping critical wind speed was calculated for a slope of the transverse force coefficient $A_1 = dC_{Fy}/d\alpha(0) = 4.9$ (Figure 5).

#	n_0 [Hz]	ρ [kg/m^3]	M [kg]	ζ_0 [%]	m^* [-]	Sc [-]	U_g/U_r [-]	Re_r [-]
D77-1_1	9.04	1.21	5.526	0.045	6.4e-04	2.9	0.19	33,700
D77-1_2	9.26	1.20	5.228	0.084	6.7e-04	5.1	0.34	34,500
D77-1_3	9.26	1.22	5.228	0.10	6.8e-04	6.0	0.40	34,500
D77-1_4	9.27	1.22	5.228	0.12	6.8e-04	7.2	0.48	34,600
D77-1_5	9.05	1.22	5.526	0.15	6.5e-04	9.5	0.63	33,700
D77-1_6	9.05	1.22	5.526	0.26	6.4e-04	16.8	1.12	33,700
D77-1_7	9.06	1.22	5.526	0.44	6.5e-04	28.0	1.86	33,800
D77-1_8	9.02	1.22	5.526	0.57	6.5e-04	36.2	2.40	33,600
D77-1_9	9.02	1.21	5.526	0.64	6.4e-04	41.4	2.75	33,600
D77-1_10	9.04	1.23	5.526	0.71	6.5e-04	45.0	2.99	33,700
D77-1_11	9.01	1.19	5.526	0.88	6.3e-04	57.8	3.83	33,600
D77-1_12	9.01	1.20	5.526	1.35	6.3e-04	87.7	5.82	33,600
D77-1_13	9.02	1.21	5.526	2.40	6.4e-04	154.8	10.27	33,600

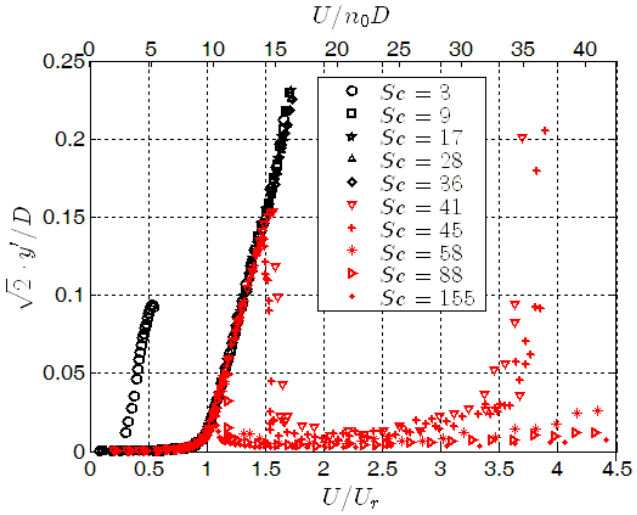

Figure 9. Amplitude-velocity curves measured in the wind tunnel in smooth flow for the larger plywood rectangular cylinder (D = 77 mm) for various damping coefficients.

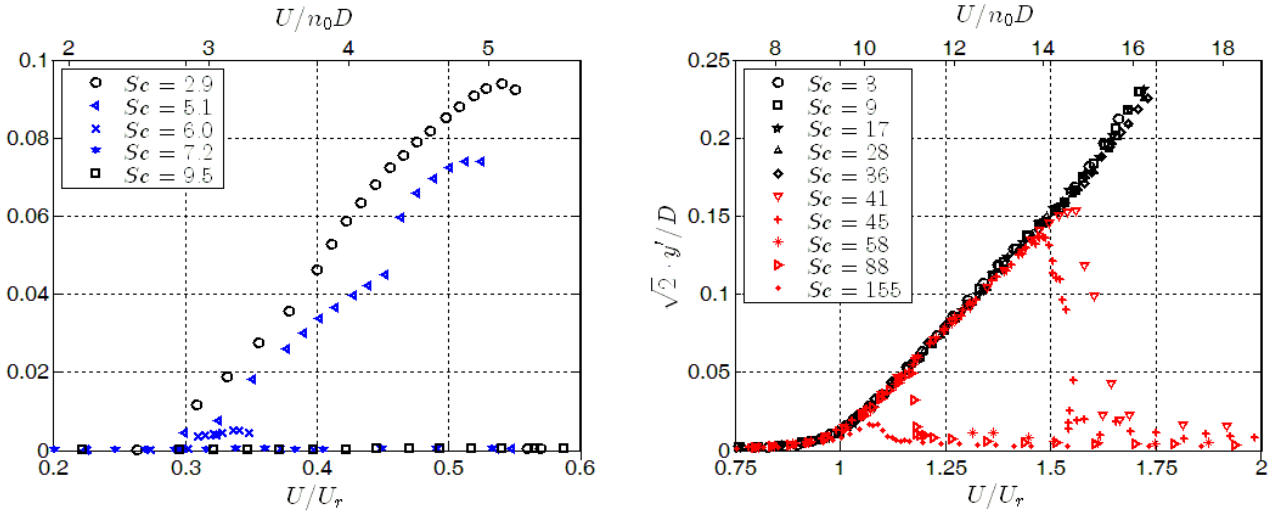

(a) (b)

Figure 10. Close-up views of the amplitude-velocity curves (see also Figure 9) in the superharmonic-resonance range (a) and around the main resonance range (b).

3.3 Aeroelastic results in smooth flow for varying Scruton number

For the larger plywood model in smooth flow, the analysis was extended by studying the effect of progressively increasing the Scruton number up to high values. The dissipation capability of the system was varied in a controlled way by introducing external viscous mechanical damping through magnetic damper devices. The tested configurations with all the dynamic parameters are listed in Table 3. Figure 9 and Figure 10 show the results in terms of amplitude-velocity curves.

For Scruton numbers up to about 6, one can notice a superharmonic resonance of order 3, always starting at a wind speed around $U_r/3$ but with the peak amplitude and the width of the range of excitation quickly reducing by increasing the system damping. Perfectly harmonic vibrations at the system natural frequency were observed in this region with amplitudes up to nearly $0.1 \cdot D$ (Figure 11).

Around the main resonance region, the response for all the Scruton numbers tested followed the same pattern, with non-negligible oscillations appearing slightly before $U = U_r$ and then increasing with the wind speed with a linear trend. For Scruton numbers up to about 36, the amplitude of oscillation (at a frequency of about $0.98\text{-}0.99 \cdot n_0$) continued growing with the flow speed up to the limit imposed by the experimental rig. In particular, for the smallest Sc values a slight increase in the slope of the response curve can be noticed for $U > 1.5 \cdot U_r$. By contrast, for Scruton numbers higher than about 41, the oscillations suddenly decrease down to very low values around U/U_r = 1.5. By further increasing the Scruton number, the velocity at which the excitation ceases progressively decreases, although the growing branch of the response remains the same. For a Scruton number value of 88 the peak response amplitude is still about $0.05 \cdot D$, while for Sc = 155 it is reduced to about $0.015 \cdot D$. It is worth noting that the time histories of the response show significant amplitude modulations (Figure 12), typical of quasi-periodic galloping (see *e.g.* Refs. [12-14]) up to about U/U_r = 1.5. Beyond this limit, the oscillations tend to become harmonic.

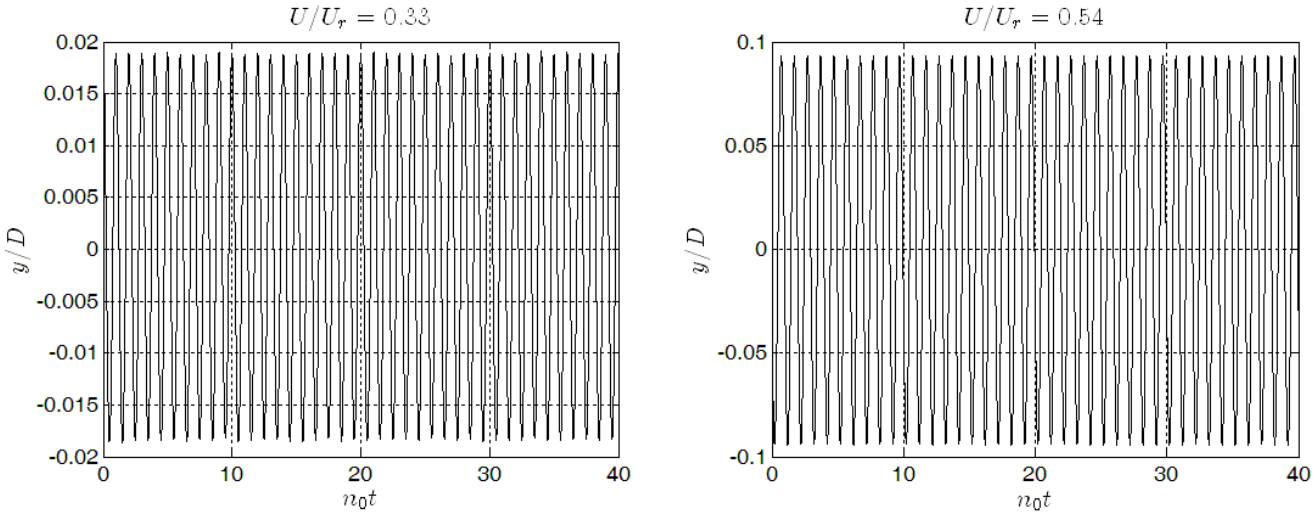

Figure 11. Examples of displacement time histories in the superharmonic resonance range.

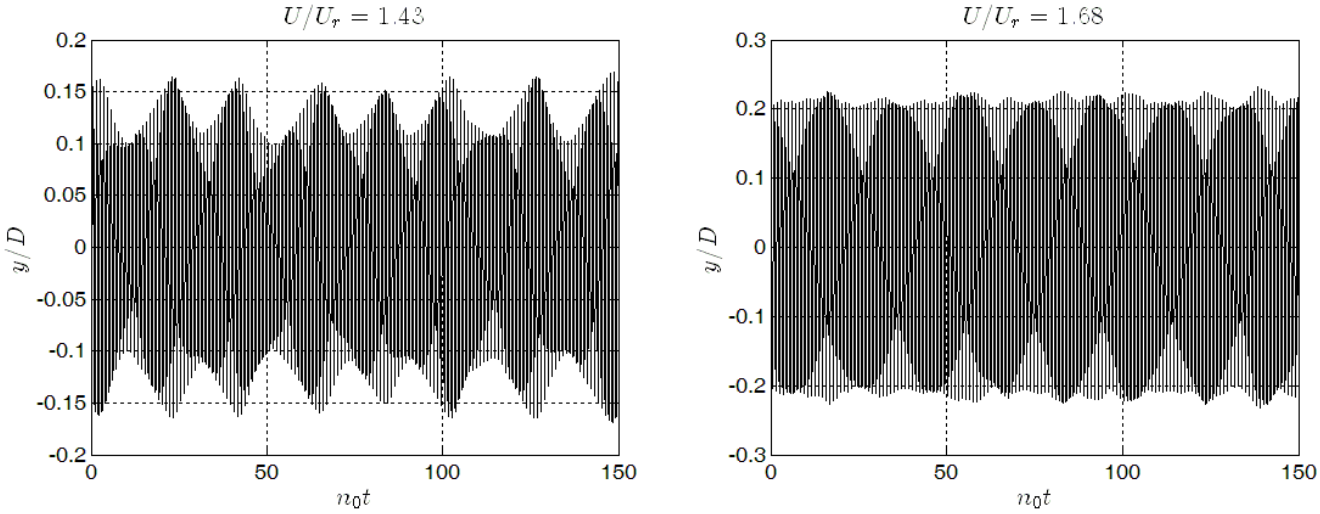

Figure 12. Examples of displacement time histories for the main instability branch.

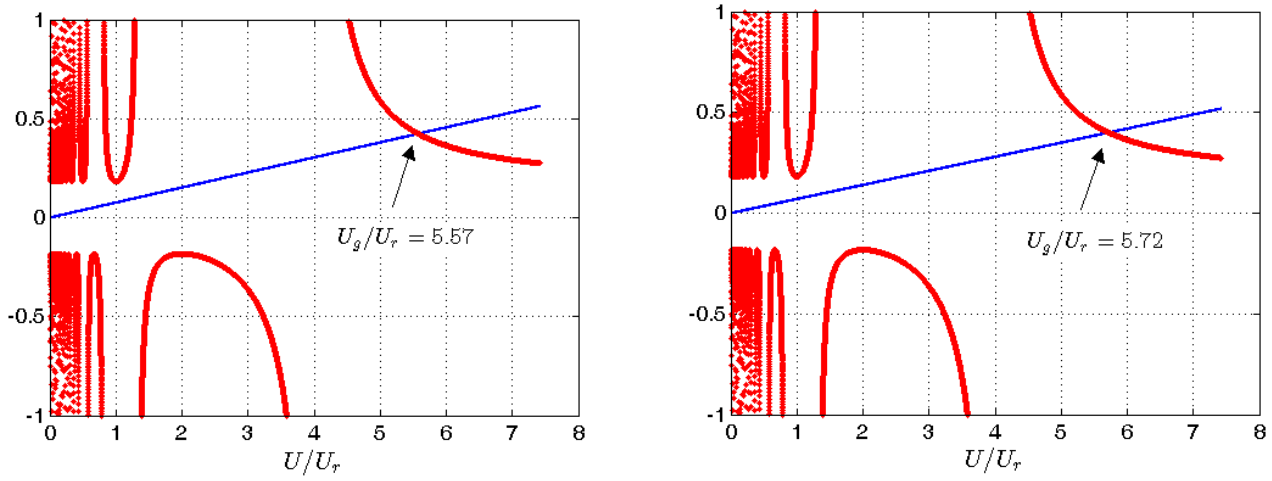

(a) (b)

Figure 13. Calculation of the galloping critical wind speed with the quasi-steady theory modified by accounting for a time delay equal to the period of vortex shedding (see Ref. [16]): (a) test case D77-1_8 (Sc = 41.4); (b) test case D77-1_9 (Sc = 45.0). A slope of the transverse force coefficient $A_1 = dC_{Fy}/d\alpha(0) = 5.5$, corresponding to high-Reynolds-number static force measurements (see Figure 5), was considered here.

In two cases (D77-1_8 with Sc = 41.4 and D77-1_9 with Sc = 45.0), wherein separation of VIV and galloping excitations occurred, it was also possible to observe in the wind tunnel the onset of galloping oscillations (Figure 9). Nevertheless, despite these occurred at high reduced wind speed (in both cases U/n_0D was around 35, that is U/U_r between 3.5 and 4), the critical threshold resulted to be significantly delayed as compared to the quasi-steady theory predictions. In fact, as shown in Table 3, the latter were estimated to be U_g/U_r = 2.75 and 2.99 respectively for test cases D77-1_8 and D77-1_9, considering A_1 = 4.9; or even U_g/U_r = 2.44 and 2.65 if the more appropriate high-Reynolds number value A_1 = 5.5 (Figure 5) is assumed in the calculations. This discrepancy can be explained by considering that a significant non-zero phase angle between the transverse force and the body displacement velocity can persist up to very high reduced wind speed, as show in Ref. [15] in the case of a square cylinder. Figure 13 shows that galloping critical wind speeds even higher than those measured in the wind tunnel can be obtained by assuming a time delay equal to a period of vortex shedding, as suggested by Hémon [16].

4 CONCLUDING REMARKS AND OUTLOOK

The experiments on a rectangular 3:2 cylinder showed that the galloping instability, either interacting with vortex shedding or not, is delayed by turbulence to higher flow speeds but the section became stable in the wind-tunnel range of flow speeds only for high turbulence intensity and large integral length scale. The actual mechanism with which turbulence tends to stabilize the system has not been understood yet. Indeed, static tests in turbulent flow are planned to this purpose.

Moreover, the qualitative discrepancy in the behaviors of the plywood and aluminum models also requires further investigation. In particular, aeroelastic tests increasing the Scruton number by means of magnetic damper devices will be repeated soon in various turbulent flows.

REFERENCES

[1] C. Mannini, A.M. Marra and G. Bartoli, VIV-galloping instability of rectangular cylinders: Review and new experiments, *Journal of Wind Engineering and Industrial Aerodynamics* 132, 109-124, 2014.

[2] C. Mannini, A.M. Marra and G. Bartoli, Experimental investigation on VIV-galloping interaction of a rectangular 3:2 cylinder, *Meccanica* 50 (3), 841-853, 2015.

[3] C. Mannini, A.M. Marra and G. Bartoli, VIV and galloping instability of a rectangular cylinder with a side ratio of 1.5, *Proceedings of the 9th European Conference on Structural Dynamics*, Porto, Portugal, 2014.

[4] C. Mannini, T. Massai, A.M. Marra and G. Bartoli, Modelling the interaction of VIV and galloping for rectangular cylinders, *Proceedings of the 14th International Conference on Wind Engineering*, Porto Alegre, Brazil, 2015.

[5] C.F. Cowdrey, A note on the use of end plates to prevent three-dimensional flow at the ends of bluff cylinders, *Aeronautical Research Council*, Current Paper No. 683, HMSO, London, 1963.

[6] A. Laneville, *Effects of turbulence on wind induced vibrations of bluff cylinders*, Ph.D. thesis, Vancouver, Canada, University of British Columbia, 1973.

[7] G.V. Parkinson and N.P.H. Brooks, On the aeroelastic instability of bluff cylinders, *Journal of Applied Mechanics* 28 (2), 252-258, 1961.

[8] G.V. Parkinson and J.D. Smith, The square prism as an aeroelastic non-linear oscillator, *Quarterly Journal of Mechanics and Applied Mathematics* 17 (2), 225-239, 1964.

[9] M. Novak and A.G. Davenport, Aeroelastic instability of prisms in turbulent flow, *Journal of Engineering Mechanics Division* 96 (1), 17-39, 1970.

[10] A. Laneville and G.V. Parkinson, Effects of turbulence on galloping of bluff cylinders, *Proceedings of the 3rd International Conference on Wind Effects on Buildings and Structures*, Tokyo, Japan, 787-797, 1971.

[11] Y. Nakamura and Y. Ohya, The effects of turbulence on the mean flow past two-dimensional rectangular cylinders, *Journal of Fluid Mechanics* 149, 255-273, 1984.

[12] A. Luongo, D. Zulli, Parametric, external and self-excitation of a tower under turbulent wind flow, *Journal of Sound and Vibration* 330 (13), 3057-3069, 2011.

[13] I. Kirrou, L. Mokni, M. Belhaq, On the quasiperiodic galloping of a wind-excited tower, *Journal of Sound and Vibration* 332 (18), 4059-4066, 2013.

[14] I. Kirrou, L. Mokni, M. Belhaq, Quasiperiodic galloping of a wind-excited tower near secondary resonances of order 2, *Journal of Vibration and Control* (in press).

[15] L. Carassale, A. Freda and L. Banfi, Qualitative analysis of the motion-excited forces acting on a square cylinder, *Proceedings of the 13th Conference of the Italian Association for Wind Engineering*, Genoa, Italy, 2014.

[16] P. Hémon, Modélisation de l'interférence de galop de cylindres circulaires en écoulement transverse, *Comptes Rendus de l'Académie des Sciences - Séries IIB - Mechanics-Physics-Chemistry-Astronomy* 324 (10), 611-618, 1997 (in French).